ACS OMEGA

http://pubs.acs.org/journal/acsodf

Article

# Finding New Precursors for Light Harvesting Materials: A Computational Study of the Fluorescence Potential of Benzanthrone Dyes

Yasir Altaf,* Sana Ullah, Farhan A. Khan, Aneela Maalik, Syeda Laila Rubab, and Muhammad Ali Hashmi*

Cite This: *ACS Omega* 2021, 6, 32334−32341

Read Online

ACCESS | Metrics & More | Article Recommendations | Supporting Information

**ABSTRACT:** Benzanthrone dyes are organic luminophores with excellent optoelectronic properties. This computational investigation is based on density functional theory and aims to explore the photophysical behavior of some of the reported aminobenzanthrones in addition to many unreported dyes containing different electron-donating substituents. Significant changes in the dipole moment and the overall structure of the dyes upon solvation in ethanol have been observed. We find that intramolecular charge transfer is more pronounced in the solvent medium, which facilitates the emission to shift bathochromically. Intersystem crossing is predicted to be absent, which makes relaxation of the molecule to ground state more efficient by emitting in the visible region.

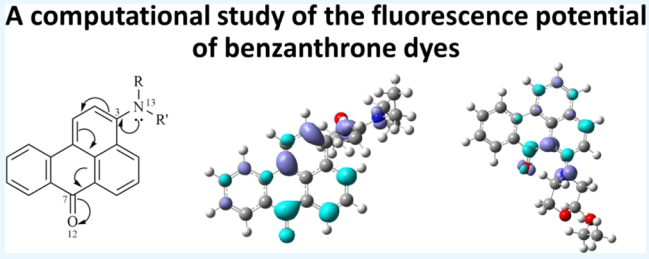


## INTRODUCTION

Benzanthrone (Scheme 1) dyes are organic luminescent materials that have emission spectra anywhere from the green to the red spectral region.[1] They are well known for having extended $\pi$-conjugation that endowed these compounds with interesting photophysical and photochemical characteristics[2−4] and excellent luminescence[5,6] and, more precisely, fluorescence[7−9] properties.

**Scheme 1. Benzanthrone**

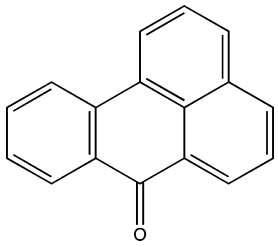

In recent years, 3-substituted benzanthrone derivatives gained attraction due to their potential applications in optoelectronic and liquid-crystalline materials.[9−18] The leading contribution by Gonta and co-workers reported the synthesis of a range of benzanthrone 3-amidines and studied their absorption and emission spectra.[8] The absorption was reported at 410−490 nm with high Stokes shift (S.S.) emissions at 505−665 nm.

Apart from their potential applications in optoelectronics, benzanthrone dyes also act as potential fluorescent probes for membranes[10] and biomolecules.[11] Ryzhova *et al.* reported such benzanthrone probes with applications in membrane and protein studies.[19] The effect of the carbonyl group appears to render the attachment of amino and alkoxy nucleophiles possible on the benzanthrone nucleus as evident from the above examples. This electron flow from the substituents to the benzanthrone nucleus gives rise to donor−acceptor interactions that can be exploited spectroscopically.

Potential applications of benzanthrone dyes in fluorescent materials have encouraged the exploration of the physical and photophysical parameters of these molecules. Kapusta *et al.* explained the dependency of intersystem crossings (ISCs) with respect to solvent and substituent effects in benzanthrone dyes.[20] Based on a mixture of experimental and quantum chemical evidence, it has been suggested that the activation energy barrier for singlet to triplet state transition increases with the increasing polarity of the solvent. Another computational study tried to make predictions based on the dipole moment and HOMO and LUMO energies of benzanthrone dyes.[18] However, because of the relatively low computational effort, the dipole moments were likely overestimated, which made conclusive

**Received:** October 19, 2021
**Accepted:** November 3, 2021
**Published:** November 17, 2021





https://doi.org/10.1021/acsomega.1c05849
*ACS Omega* 2021, 6, 32334−32341

**Table 1. Comparison of Theoretical Results Using Different Methods of TD-DFT (PBE0 and CAM-B3LYP Functionals) with the Available Experimentally Reported Values of Few of the Selected Dyes (1−4)[a]**

| | $\Delta E_{abs}$ | | | $\Delta E_{ems}$ | | |
|---|---|---|---|---|---|---|
| | experimental | PBE0 | CAM-B3LYP | experimental | PBE0 | CAM-B3LYP |
| (**1**) | 455.40[31] | 533.54(17) | 471.06(3) | 640.0031 | 628.03(2) | 560.79(12) |
| (**2**) | 460.00[22] | 477.02(4) | 425.48(8) | 635.0022 | 588.64(7) | 548.38(14) |
| (**3**) | 460.00[22] | 527.88(16) | 453.66(2) | 625.0022 | 607.56(3) | 560.61(10) |
| (**4**) | 460.00[22] | 483.81(5) | 417.58(9) | 630.0022 | 592.41(6) | 548.81(13) |

[a] $\Delta E_{abs}$ is the (vertical) excitation energy and $\Delta E_{ems}$ is for emission, both expressed in nanometers. The relative percent error is given in parentheses.

predictions impossible. Similar studies have tried investigations along the same lines.[8] All these studies revolve around position-3 of the benzanthrone framework, and no significant mentioning of its derivatives involving other positions is available in the literature.

In order to gain a deeper understanding of the fluorescence property of benzanthrone dyes with substituents on different positions of the benzanthrone framework, a detailed investigation of the characteristics of the excited states would be necessary. Computational chemistry has been successful in explaining the excited-state properties of various systems through time-dependent density functional theory (DFT).[21] However, to the best of our knowledge, there is no evidence of a comprehensive study using computational tools to explore the excited-state properties of benzanthrone dyes with substitution at different positions of the benzanthrone framework. The current work is an attempt to gain insight into the absorption and emission phenomena taking place in benzanthrone dyes. Previously synthesized 3-aminobenzanthrone derivatives that were reported elsewhere[22] as fluorescent have been selected for this purpose. Additionally, other compounds with substitution over different positions are included to observe their absorption and emission.

## COMPUTATIONAL DETAILS

All calculations were carried out with the Gaussian 09 suite of programs (Revision D.01)[23] using DFT. The range-separated hybrid CAM-B3LYP functional[24] and the PBE0 hybrid functional[25−27] in conjunction with Grimme's empirical D3 correction including Becke−Johnston damping (D3BJ)[28,29] were benchmarked using the def2-TZVP basis set[30] of triple-$\zeta$ quality for the experimentally reported results (Table 1). Although both the functionals performed well overall, it may be observed that there is a greater accuracy in results with PBE0 in most of the cases. Hence, we proceeded with the PBE0-D3BJ/def2TZVP method for our calculations and underlying discussion. One may get a mixed feeling of accuracy in the case of vertical excitations with both the functionals; therefore, these calculations will be performed using PBE0 as well as CAM-B3LYP for all the molecules of interest.

Gas-phase geometry optimization of all the molecules was performed to identify equilibrium structures. Frequency calculations were carried out to ensure that the obtained structures are true minima on the potential energy surface. Subsequent time-dependent DFT (TD-DFT) excited-state calculations at the previously obtained geometries were carried out to determine the vertical excitation spectra. Natural transition orbitals (NTOs) were calculated in order to compute density difference maps between ground and (vertically) excited state. Excited-state optimizations were then carried out followed by ground-state single-point calculations at the obtained geometries in order to calculate the emission spectrum. To investigate the solvent effects,[29] the calculations were repeated with the SMD solvent model established by Cramer and Truhlar[31] by explicitly adding one solvent molecule in all the cases. Since the experimental data were obtained in ethanol,[22] the calculations used the parameter set for the same solvent.

Molecular graphics were rendered with GaussView 5.0.9.[32]

## RESULTS AND DISCUSSION

It has been suggested earlier that intramolecular charge transfer is mainly responsible for the fluorescence characteristics of 3-aminobenzanthrone dyes.[22] Upon excitation, the electron-donating groups attached to the 3-position of the benzanthrone nucleus transfer electron density to the electrophilic carbonyl group (Scheme 2).[7] This results in absorption in the visible region.

**Scheme 2. Proposed Charge-Transfer Mechanism in Benzanthrone Dyes**

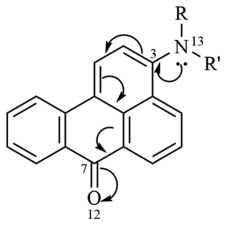


It was argued that upon excitation, the proton-accepting potential of these dyes increases, which changes the hydrogen bonding network.[33] As a result, the $\pi \rightarrow \pi^*$ transition becomes feasible, which subsequently causes fluorescence. Obviously, this effect can be amplified or attenuated in a polar solvent. In a less polar medium, the solvent molecules have fewer dipole−dipole interactions with the solute, thereby decreasing the observed fluorescence. However, more polar solvents increase the described effect and, in turn, fluorescence.[34]

The fluorescence spectra (in ethanol) and applications in the membrane studies of the benzanthrone dyes (**1**−**4**) were reported by Trusova *et al.*[22] However, other molecules with different possibilities of substitution on the benzanthrone framework (**5**−**16**) have also been added to better understand the absorption and emission in benzanthrone dyes. For a detailed discussion, we have divided our contribution into three parts, *viz*, ground-state structures, vertical excitations, and the structure of the excited state for each of these molecules.

**Ground-State Structures.** A comparison of some structural features for the ground-state geometries optimized in the gas phase and in ethanol is given in Table 2. Although, to the best of our knowledge, none of the dyes in this study have been characterized crystallographically, our calculated C═O bond


https://doi.org/10.1021/acsomega.1c05849
ACS Omega 2021, 6, 32334−32341

Table 2. Key Parameters from the Ground-State Structures Both in the Gas Phase and in the Solvent at the PBE0-D3(BJ)/def2-TZVP Level[a]

| | gas phase | | ethanol | |
|---|---|---|---|---|
| | CO | $\mu$ | CO | $\mu$ |
| (1) | 1.22 (1.22) | 5.2 (4.8) | 1.24 (1.23) | 9.6 (11.6) |
| (2) | 1.22 (1.22) | 7.3 (7.2) | 1.23 (1.23) | 11.3 (12.7) |
| (3) | 1.22 (1.22) | 7.2 (8.1) | 1.23 (1.23) | 11.1 (16.7) |
| (4) | 1.22 (1.22) | 7.6 (7.4) | 1.23 (1.23) | 11.6 (10.7) |
| (5) | 1.23 (1.22) | 3.0 (3.1) | 1.24 (1.23) | 3.2 (3.3) |
| (6) | 1.22 (1.22) | 2.5 (2.5) | 1.24 (1.23) | 5.6 (5.9) |
| (7) | 1.22 (1.22) | 4.6 (4.5) | 1.23 (1.23) | 8.6 (7.7) |
| (8) | 1.22 (1.22) | 6.4 (6.2) | 1.24 (1.23) | 12.9 (12.5) |
| (9) | 1.22 (1.22) | 3.4 (3.4) | 1.24 (1.23) | 7.0 (6.9) |
| (10) | 1.22 (1.22) | 5.9 (5.6) | 1.23 (1.23) | 8.2 (7.3) |
| (11) | 1.22 (1.22) | 5.9 (5.6) | 1.24 (1.23) | 13.4 (13.0) |
| (12) | 1.23 (1.22) | 4.6 (4.5) | 1.24 (1.23) | 5.1 (4.7) |
| (13) | 1.22 (1.22) | 4.6 (4.3) | 1.23 (1.23) | 8.6 (8.4) |
| (14) | 1.24 (1.23) | 2.1 (2.1) | 1.25 (1.24) | 5.9 (6.0) |
| (15) | 1.24 (1.23) | 3.6 (3.2) | 1.25 (1.25) | 6.2 (5.5) |
| (16) | 1.22 (1.22) | 5.0 (4.7) | 1.23 (1.23) | 9.5 (8.9) |

[a]The results calculated using CAM-B3LYP are given in parentheses. CO refers to the length of the C7=O12 double bond, the carbonyl functionality of benzanthrone. $\mu$ shows the dipole moment of the compound in question and is given in debye.

length matches the bond length of a recently reported crystal structure of a different benzanthrone derivative.[31] As expected for aromatic ketones, the C═O bond length is not affected much by changing different substituents. However, there appears a minute elongation in C═O bond length from gas to solvent phase, which may be attributed to the combined effect of hydrogen bonding with the ethanol solvent and the intramolecular charge transfer in the solvent phase. All the 16 compounds are significantly polar as suggested by the dipole moment. The dipole moment increases to a great extent in ethanol solvent (Table 2).

**Vertical Excitations.** The energy of the first vertical excitation, their oscillator strength, and the dipole moment for the same state are given in Table 3. The oscillator strength ($f$) corresponds to the intensity of absorption here. The higher the $f$ value, the stronger the absorption will be.

It is evident from the table that all the molecules are highly absorbent in the gas phase and that their absorptivity still increases in the solution. However, it is the highest for (7) with a value of 0.87 for its oscillator strength in ethanol, which predicts the most intense absorption peak among all the dyes. The absorption is within the range of 2.58−3.21 eV (3.10−3.59 eV with CAM-B3LYP) in the gas phase, while in solvent, their absorption ranges from 2.32 to 3.04 eV (2.63−3.39 eV with CAM-B3LYP). Generally, larger dipole moments of the excited state correspond to enhanced absorption. Our calculated excitation energies correlate well with the experimental results, with CAM-B3LYP performing a slightly better to calculate absorption energies. A maximum relative error of about 17% with PBE0 was observed compared to 9% with CAM-B3LYP, which compares well with the accuracy that has been achieved previously on similar systems, that is, 23% relative error.[35] Even though others have rationalized these error margins in terms of the assumption that a single conformer is responsible for the electronic transition (while in reality, one expects a Boltzmann weighted spectrum composed of the excitations of many

Table 3. Vertical Excitations of (1−20) at the TD-DFT PBE0-D3(BJ)/def2-TZVP Level of Theory[a]

| | gas phase | | | ethanol | | |
|---|---|---|---|---|---|---|
| | $\Delta E_{abs}$ | $f$ | $\mu$ | $\Delta E_{abs}$ | $f$ | $\mu$ |
| (1) | 2.77 (3.22) | 0.25 (0.34) | 10.1 (8.9) | 2.32 (2.63) | 0.50 (0.64) | 15.2 (19.0) |
| (2) | 2.88 (3.27) | 0.26 (0.40) | 10.5 (11.2) | 2.60 (2.91) | 0.51 (0.70) | 15.2 (18.8) |
| (3) | 2.88 (3.31) | 0.27 (0.45) | 10.6 (11.7) | 2.35 (2.73) | 0.65 (0.79) | 25.0 (23.5) |
| (4) | 2.85 (3.26) | 0.27 (0.36) | 11.0 (10.6) | 2.56 (2.97) | 0.51 (0.64) | 16.2 (14.7) |
| (5) | 2.86 (3.17) | 0.12 (0.15) | 2.4 (2.4) | 2.73 (2.99) | 0.34 (0.39) | 3.0 (3.1) |
| (6) | 2.68 (3.28) | 0.09 (0.10) | 3.5 (3.3) | 2.59 (2.84) | 0.28 (0.32) | 5.7 (5.7) |
| (7) | 3.07 (3.42) | 0.40 (0.47) | 7.6 (6.5) | 2.66 (3.09) | 0.87 (0.89) | 15.0 (11.6) |
| (8) | 3.05 (3.42) | 0.23 (0.32) | 9.6 (9.4) | 2.63 (2.96) | 0.47 (0.60) | 18.2 (17.9) |
| (9) | 3.05 (3.42) | 0.00 (0.00) | 1.8 (1.9) | 3.04 (3.31) | 0.46 (0.56) | 8.2 (8.3) |
| (10) | 2.88 (3.33) | 0.16 (0.21) | 10.9 (9.4) | 2.54 (3.00) | 0.40 (0.50) | 15.8 (13.2) |
| (11) | 3.21 (3.57) | 0.10 (0.09) | 5.6 (4.8) | 2.82 (3.10) | 0.48 (0.58) | 16.7 (16.8) |
| (12) | 2.97 (3.29) | 0.14 (0.18) | 4.5 (4.4) | 2.83 (3.08) | 0.41 (0.48) | 6.4 (5.9) |
| (13) | 2.91 (3.39) | 0.22 (0.31) | 11.08 (8.3) | 2.57 (3.02) | 0.48 (0.62) | 16.8 (14.9) |
| (14) | 2.58 (3.09) | 0.21 (0.32) | 6.8 (5.5) | 2.31 (2.75) | 0.49 (0.64) | 10.9 (9.8) |
| (15) | 2.60 (3.10) | 0.30 (0.41) | 2.2 (2.0) | 2.32 (2.75) | 0.66 (0.78) | 7.3 (6.5) |
| (16) | 3.09 (3.59) | 0.09 (0.00) | 14.1 (3.6) | 2.81 (3.39) | 0.38 (0.46) | 20.2 (11.4) |

[a]The values calculated with the CAM-B3LYP functional are given in parentheses. $\Delta E_{abs}$ is the (vertical) excitation energy in eV, $f$ is the oscillator strength (which correlates with absorptivity), and $\mu$ is the dipole moment of first excited state in debye.

conformers with more or less similar excitation energies), we believe that the error in this investigation is a reflection of the fundamental limitations of approximate DFT in the TD-DFT framework. In our view, the relatively rigid benzanthrone moiety does not lend itself to the generation of a large conformational space.

**NTO Analysis.** As discussed above, benzanthrone derivatives are said to fluoresce because of the intramolecular charge transfer. In order to develop a detailed understanding of this phenomenon, we analyzed the NTOs for the vertical excitations discussed above. The NTO analysis simplifies a qualitative description of an electronic transition by optimizing a "particle" and a "hole" orbital that allow the excitation to be represented in the one-particle picture—as a transition between those two orbitals. Figure 1 shows the density difference between these two orbitals of **4** and hence charge transfer upon excitation. The areas of charge depletion are shown in DARK-BLUE, while the areas of charge accumulation are shown in LIGHT-BLUE. It can be clearly seen that the charge density on the terminal nitrogen (right side) is transferred to the benzanthrone moiety. The charge transfer is also more pronounced in ethanol when compared to the gas phase.

There are many other smaller differences in both phases if we look at the structures in Figure 1. For instance, the charge depletion from C9, C2−C3, and C11″−C3″ (atom numbering



https://doi.org/10.1021/acsomega.1c05849
ACS Omega 2021, 6, 32334−32341

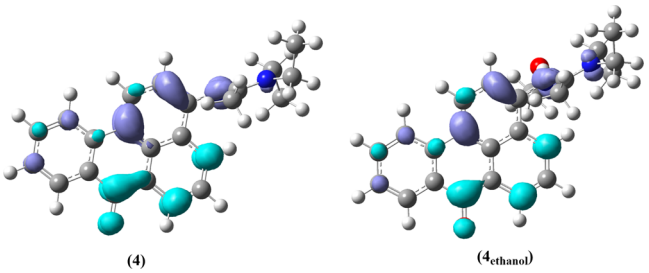


**Figure 1.** Illustration of charge transfer after a vertical excitation of **4**. Areas of charge depletion are indicated in dark blue, and areas of charge accumulation are indicated in light blue.

according to Scheme 3) is higher in the gas-phase structure compared to that in ethanol, which is again an indication of enhanced charge transfer from the substituent toward the carbonyl group in solvated form. All the other molecules follow the same pattern of intramolecular charge transfer from substituent(s) to the benzanthrone framework. However, in the case of dyes **5**−**7**, **10**, and **12**, the NTO plots of both gas and solvent phases show charge depletion over the benzanthrone framework, more significantly the ketonic oxygen. It is evident in the NTO analysis of **5** as shown in Figure 2 that O7, C11″, and C3′ of benzanthrone framework are marked with charge depletion. This seems to affect their emission, which will be explained in next section.

**Structure of the Excited State.** Table 4 indicates data for excited-state optimization of benzanthrone dyes under investigation in the gas phase and in ethanol. All the emission peaks are consistent with the experimental results. The reported $\Delta E_{ems}$ for (**1**−**4**) is in the range of 625−640 nm.[22] The calculated $\Delta E_{ems}$ is 1.97 eV (628.03 nm), 2.11 eV (588.64 nm), 2.04 eV (607.56 nm), and 2.09 eV (592.41 nm) for **1**, **2**, **3**, and **4**, respectively, with a maximum error of about 7%. The difference between dipole moment is highly marked between the gas-phase

**Scheme 3. Benzanthrone Dyes in the Current Investigation**[a]

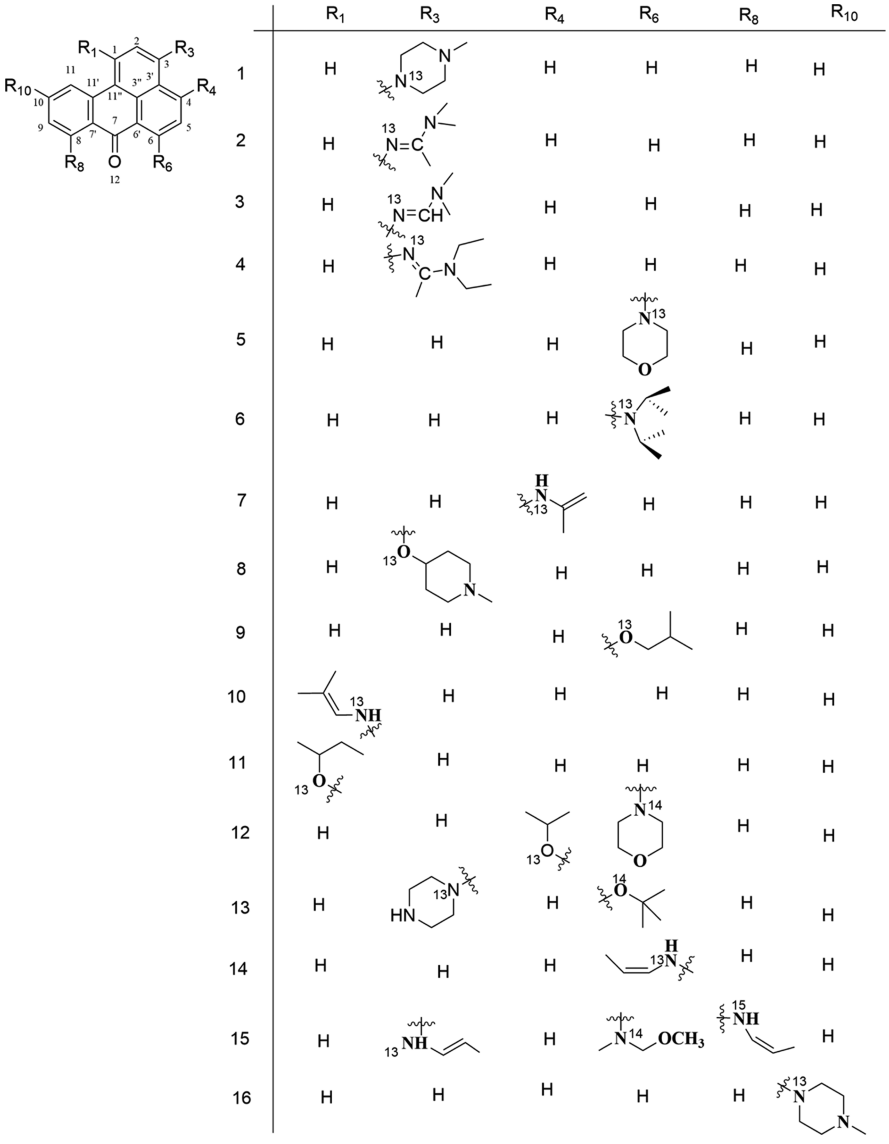


[a]Compounds (**1**−**4**) are experimentally reported elsewhere, while compounds (**5**−**20**) are absent from the literature. The atomic numbering is also used to refer to specific molecular locations in the discussion.



https://doi.org/10.1021/acsomega.1c05849
ACS Omega 2021, 6, 32334−32341

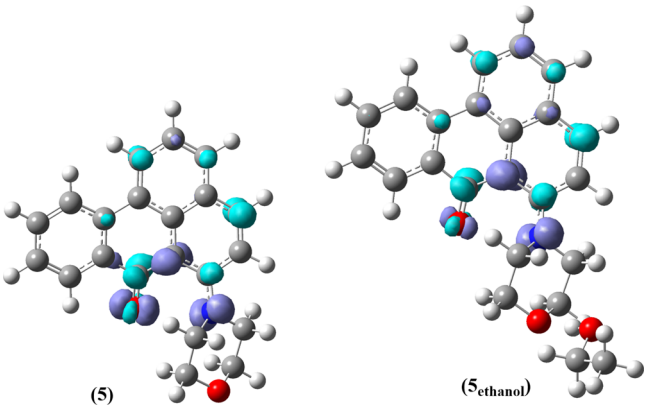


**Figure 2.** Illustration of the charge transfer after a vertical excitation of **5**. Areas of charge depletion are indicated in dark blue, and areas of charge accumulation are indicated in light blue.

**Table 4. Results of Excited-State Optimization Highlighting the Energy Emitted ($\Delta E_{ems}$) in eV, Oscillator Strength ($f$), and Dipole Moment ($\mu$) in Debye for the First Excited State**

| | gas phase | | | ethanol | | |
|---|---|---|---|---|---|---|
| | $\Delta E_{ems}$ | $f$ | $\mu$ | $\Delta E_{ems}$ | $f$ | $\mu$ |
| (**1**) | 2.39 | 0.21 | 6.2 | 1.97 | 0.47 | 14.5 |
| (**2**) | 2.40 | 0.24 | 8.6 | 2.11 | 0.52 | 12.6 |
| (**3**) | 2.45 | 0.25 | 8.3 | 2.04 | 0.63 | 20.2 |
| (**4**) | 2.36 | 0.25 | 8.9 | 2.09 | 0.53 | 13.1 |
| (**5**) | 0.83 | 0.00 | 5.2 | 0.97 | 0.00 | 7.6 |
| (**6**) | 0.84 | 0.00 | 3.6 | 0.98 | 0.00 | 7.8 |
| (**7**) | 1.68 | 0.00 | 3.4 | 1.83 | 0.00 | 7.2 |
| (**8**) | 2.63 | 0.19 | 7.2 | 2.30 | 0.42 | 14.6 |
| (**9**) | 2.15 | 0.00 | 3.7 | 2.66 | 0.42 | 9.2 |
| (**10**) | 1.37 | 0.00 | 3.7 | 1.35 | 0.00 | 5.3 |
| (**11**) | 2.68 | 0.00 | 6.7 | 2.47 | 0.42 | 14.4 |
| (**12**) | 1.00 | 0.00 | 5.3 | 1.12 | 0.00 | 5.5 |
| (**13**) | 1.71 | 0.00 | 4.1 | 2.09 | 0.45 | 12.2 |
| (**14**) | 0.91 | 0.00 | 5.2 | 1.84 | 0.39 | 7.7 |
| (**15**) | 1.89 | 0.18 | 6.3 | 1.94 | 0.65 | 8.9 |
| (**16**) | 2.54 | 0.07 | 5.0 | 2.37 | 0.36 | 9.1 |

and the corresponding ethanol-phase structures, which shows significant polarization of all the molecules in ethanol.

In gas-phase comparison of the optimized geometry of the excited state to that of the solvated phase, the highest increase in dipole moment has been recorded for **2**, that is, 11.9 D. As discussed earlier, this increase in polarity can be attributed to the polar solvent, which facilitates intramolecular charge transfer possibly by making hydrogen bonds with O and N present in the dyes. The oscillator strength ($f$) also increases in most of the dyes except few while moving from the gas phase to the solvent medium. This value is the highest for compound **15**. In the case of the experimentally reported first four dyes, **3** has the highest oscillator strength, which is in line with the most intense emission peak of all the four reported in the fluorescence spectrum.[22]

It may be observed in Table 4 that a very low intensity of emission for compounds **5**−**7**, **10**, and **12** is indicated by the oscillator strength ($f$) for these dyes. This may be attributed to the charge depletion from carbonyl oxygen of the benzanthrone framework during their vertical excitation (Figure 2) opposite to the rest of the molecules where charge accumulation on carbonyl oxygen takes place (Figure 1) as a result of vertical excitation. Interestingly, these five compounds have emission maxima in the near-infrared region with **7** and **10** emitting in the near-infrared fluorescence (NIRF) region (650−950 nm). This property makes **7** and **10** potential candidates in NIRF imaging because of the absorption by the body cells and hence low scattering of light emitted in this region[36] that makes the targeted molecule more visible.

The S.S. can be calculated as the difference between the absorbed energy, upon vertical excitation, and the emission energy, resulting from relaxation of the excited-state minimum back to the ground state. These are given in Table 5 along with

**Table 5. Calculation of S.S. of the Dyes of Interest[a]**

| | $\Delta E_{abs}$ | $\mu_{abs}$ | $\Delta E_{ems}$ | $\mu_{ems}$ | S.S. |
|---|---|---|---|---|---|
| (**1**) | 2.32 | 15.2 | 1.97 | 14.5 | 0.35 |
| (**2**) | 2.60 | 15.2 | 2.11 | 12.6 | 0.49 |
| (**3**) | 2.35 | 23.5 | 2.04 | 20.2 | 0.31 |
| (**4**) | 2.56 | 14.7 | 2.09 | 13.1 | 0.47 |
| (**5**) | 2.73 | 3.0 | 0.97 | 7.6 | *1.76* |
| (**6**) | 2.59 | 5.7 | 0.98 | 7.8 | *1.61* |
| (**7**) | 2.66 | 15.0 | 1.83 | 7.2 | *0.83* |
| (**8**) | 2.63 | 18.2 | 2.30 | 14.6 | 0.33 |
| (**9**) | 3.04 | 8.2 | 2.66 | 9.2 | 0.38 |
| (**10**) | 2.54 | 15.8 | 1.35 | 5.3 | *1.19* |
| (**11**) | 2.82 | 16.7 | 2.47 | 14.4 | 0.35 |
| (**12**) | 2.83 | 6.4 | 1.12 | 5.5 | *1.71* |
| (**13**) | 2.57 | 16.8 | 2.09 | 12.2 | 0.48 |
| (**14**) | 2.31 | 10.9 | 1.84 | 7.7 | 0.47 |
| (**15**) | 2.32 | 7.3 | 1.94 | 8.9 | 0.38 |
| (**16**) | 2.81 | 20.2 | 2.37 | 9.1 | 0.44 |

[a]S.S. for the dyes emitting in the near-infrared region are marked in italics. The dipole moment of ethanol-solvated dyes on their absorption maxima $\mu_{abs}$ and, after relaxation of the excited states, to their minima $\mu_{ems}$ is also given. Energies in eV, dipole moments in debye.

the change in polarity between the absorption and emission for all the dyes. We observed high Stokes' shifts for **5**−**7**, **10**, and **12**, which may be attributed to their emission at very long wavelengths. The highest S.S. among other dyes has been observed for **2**.

**Triplet States.** A comparison of the vertical excitation in singlet and triplet states is a useful indication to predict the effect of ISC on fluorescence. One useful aspect regarding this is the comparison of the first singlet state and the lowest lying triplet state vertical excitation energies[35] as shown in Table 6. The large differences in the energy of absorption between the two states of each corresponding molecule indicate that ISC is unlikely to occur, which appears to add to the efficiency of the fluorescence characteristics in ethanol.

## CONCLUSIONS

The computational results in our current study reproduce the available experiments well. The most intense spectral peak was observed for dye **3** experimentally out of **1**−**4**, a finding which we can confirm computationally. The calculated excitation energies with the PBE0-D3BJ method have a relative error of 7% or less when compared to the experimental results except for the two deviations with 16 and 17% errors. On the other hand, the CAM-B3LYP method reproduces the results with a relative error of about 10% or more in most of the cases. Nevertheless, the results with both the functionals are well within the established


https://doi.org/10.1021/acsomega.1c05849
ACS Omega 2021, 6, 32334−32341

**Table 6. Comparison of the Excitation Energies ($\Delta E_{abs}$) in eV for the First Excited Singlet and Triplet States**

| | gas phase | | ethanol | |
|---|---|---|---|---|
| | $\Delta E_{abs,S1}$ | $\Delta E_{abs,T1}$ | $\Delta E_{abs,S1}$ | $\Delta E_{abs,T1}$ |
| (**1**) | 2.77 | 1.80 | 2.32 | 1.11 |
| (**2**) | 2.88 | 1.82 | 2.60 | 1.22 |
| (**3**) | 2.88 | 1.82 | 2.35 | 1.30 |
| (**4**) | 2.85 | 1.81 | 2.56 | 1.07 |
| (**5**) | 2.86 | 0.72 | 2.73 | 0.80 |
| (**6**) | 2.68 | 0.67 | 2.59 | 0.80 |
| (**7**) | 3.07 | 0.89 | 2.66 | 0.86 |
| (**8**) | 3.05 | 0.90 | 2.63 | 0.98 |
| (**9**) | 3.05 | 0.54 | 3.04 | 0.68 |
| (**10**) | 2.88 | 0.86 | 2.54 | 0.72 |
| (**11**) | 3.21 | 0.78 | 2.82 | 0.91 |
| (**12**) | 2.97 | 0.71 | 2.83 | 0.74 |
| (**13**) | 2.91 | 0.75 | 2.57 | 0.94 |
| (**14**) | 2.58 | 0.59 | 2.31 | 0.74 |
| (**15**) | 2.60 | 0.60 | 2.32 | 0.50 |
| (**16**) | 3.09 | 0.38 | 2.81 | 0.40 |

performance of time-dependent DFT and smaller than the 23% error that has been reported previously for similar calculations. We observed that most of the dyes in the current study are capable of emitting in the visible region except the near-infrared emission of **5**−**7**, **10**, and **12**. Compounds **7** and **10** are potential candidates in clinical applications of NIRF imaging due to their emission in the NIRF region. It has long been speculated that internal charge transfer is important in these dyes. We now show unambiguously for the first time that this is indeed the case. NTO analyses of the dyes under discussion shows how the charge flowing (specifically from the substituent) through the benzanthrone framework toward the carbonyl group is enhanced in the presence of the solvent. NTO analyses further helped us observe the charge depletion from the carbonyl oxygen of the dyes **5**−**7**, **10**, and **12** in their excited states, unlike other dyes, which may be a reason for their emission in the near-infrared region. This whole study leads us to conclude that the benzanthrone dyes under discussion are excellent candidates for optoelectronic devices, and more synthetic efforts are needed in this regard.

## ■ ASSOCIATED CONTENT

### Supporting Information

The Supporting Information is available free of charge at https://pubs.acs.org/doi/10.1021/acsomega.1c05849.

NTO plots of the experimentally known dyes (**1**−**4**) included in our studies and *xyz* coordinates of the ground-state and first excited-state geometries of compounds (**1**−**16**) (PDF)

## ■ AUTHOR INFORMATION


### Corresponding Authors

**Yasir Altaf** − *Department of Chemistry, Division of Science and Technology, University of Education Lahore, Lahore 54000, Pakistan*; Email: yasir.altaf@ue.edu.pk

**Muhammad Ali Hashmi** − *Department of Chemistry, University of Education Lahore, Attock Campus, Attock 43600, Pakistan*; orcid.org/0000-0001-5170-1016; Email: muhammad.hashmi@ue.edu.pk

### Authors

**Sana Ullah** − *Division of Science and Technology, University of Education Lahore, Lahore 54770, Pakistan*

**Farhan A. Khan** − *Department of Chemistry, COMSATS University Islamabad, Abbottabad Campus, Abbottabad 22060, Pakistan*

**Aneela Maalik** − *Department of Chemistry, COMSATS University Islamabad, Islamabad 45550, Pakistan*

**Syeda Laila Rubab** − *Department of Chemistry, Division of Science and Technology, University of Education Lahore, Lahore 54000, Pakistan*

Complete contact information is available at: https://pubs.acs.org/10.1021/acsomega.1c05849


### Notes

The authors declare no competing financial interest.

## ■ ACKNOWLEDGMENTS

The authors thank Professor Martyn Coles and Dr. Matthias Lein for their useful discussions. Additional computer time was provided by the Victoria University of Wellington High Performance Computer Facilities Heisenberg and Raapoi and by the New Zealand eScience Infrastructure (NeSI) project NESI46 and NESI00395 through the Pan cluster at the Centre for eResearch at the University of Auckland.

## ■ REFERENCES


(1) Krasovitskiĭ, B. M.; Bolotin, B. M. *Organic Luminescent Materials*; Wiley-VCH, 1988.

(2) Bentley, P.; McKellar, J. F.; Phillips, G. O. The photochemistry of benz[de]anthracen-7-ones. Part I. Electronic absorption and emission spectroscopy. *J. Chem. Soc., Perkin Trans. 2* **1974**, 523−526.

(3) Bentley, P.; McKellar, J. F.; Phillips, G. O. The photochemistry of benz[de]anthracen-7-ones. Part II. Flash photolysis. *J. Chem. Soc., Perkin Trans. 2* **1975**, 1259−1262.

(4) Bentley, P.; McKellar, J. F. The photochemistry of benz[de]-anthracen-7-ones. Part III. Fluorescence quantum yield and continuous photolysis studies. *J. Chem. Soc., Perkin Trans. 2* **1976**, 1850−1854.

(5) Kirilova, E. M.; Belyakov, S. V.; Kirilov, G. K.; Kalnina, I.; Gerbreder, V. Luminescent properties and crystal structure of novel benzanthrone dyes. *J. Lumin.* **2009**, *129*, 1827−1830.

(6) Bulanovs, A.; Kirilov, G.; Fleisher, M.; Kirilova, E.; Mihailova, I. Luminescence and structural properties of thermally evaporated benzanthrone dyes thin films. *Opto-Electron. Rev.* **2013**, *21*, 227−232.

(7) Grabchev, I.; Bojinov, V.; Moneva, I. The synthesis and application of fluorescent dyes based on 3-amino benzanthrone. *Dyes Pigm.* **2001**, *48*, 143−150.

(8) Gonta, S.; Utinans, M.; Kirilov, G.; Belyakov, S.; Ivanova, I.; Fleisher, M.; Savenkov, V.; Kirilova, E. Fluorescent substituted amidines of benzanthrone: Synthesis, spectroscopy and quantum chemical calculations. *Spectrochim. Acta, Part A* **2013**, *101*, 325−334.

(9) Nepraš, M.; Machalický, O.; Šeps, M.; Hrdina, R.; Kapusta, P.; Fidler, V. Structure and properties of fluorescent reactive dyes: Electronic structure and spectra of some benzanthrone derivatives. *Dyes Pigm.* **1997**, *35*, 31−44.

(10) Zhytniakivska, O.; Trusova, V.; Gorbenko, G.; Kirilova, E.; Kalnina, I.; Kirilov, G.; Kinnunen, P. Newly synthesized benzanthrone derivatives as prospective fluorescent membrane probes. *J. Lumin.* **2014**, *146*, 307−313.

(11) Kirilova, E. M.; Kalnina, I.; Kirilov, G. K.; Meirovics, I. Spectroscopic Study of Benzanthrone 3-N-Derivatives as New Hydrophobic Fluorescent Probes for Biomolecules. *J. Fluoresc.* **2008**, *18*, 645−648.

(12) Khrolova, O. R.; Kunavin, N. I.; Komlev, I. V.; Tavrizova, M. A.; Trofimova, S. I.; Madii, V. A.; Petukhov, V. A. Spectral and

luminescence properties of phosphorylmethyl derivatives of 3-aminobenzathrone. *J. Appl. Spectrosc.* **1984**, *41*, 771−775.
(13) Wróbel, D.; Boguta, A.; Mykowska, E.; Bauman, D.; Grabchev, I. Photothermal Properties of 3-Substituted Benzanthrone Dyes. *Mol. Cryst. Liq. Cryst.* **2005**, *427*, No. 57/[369].
(14) Grabchev, I.; Moneva, I.; Wolarz, E.; Bauman, D. Fluorescent 3-oxy benzanthrone dyes in liquid crystalline media. *Dyes Pigm.* **2003**, *58*, 1−6.
(15) Bojinov, V. B.; Grabchev, I. K. Synthesis of Ethyl 3-Aryl-1-methyl-8-oxo- 8H-anthra[9,1-gh]quinoline-2-carboxylates as Dyes for Potential Application in Liquid Crystal Displays. *Org. Lett.* **2003**, *5*, 2185−2187.
(16) Staneva, D.; Vasileva-Tonkova, E.; Makki, M. S. I.; Sobahi, T. R.; Abdel-Rahman, R. M.; Asiri, A. M.; Grabchev, I. Synthesis, photophysical and antimicrobial activity of new water soluble ammonium quaternary benzanthrone in solution and in polylactide film. *J. Photochem. Photobiol., B* **2015**, *143*, 44−51.
(17) Vus, K.; Trusova, V.; Gorbenko, G.; Sood, R.; Kirilova, E.; Kirilov, G.; Kalnina, I.; Kinnunen, P. Fluorescence Investigation of Interactions Between Novel Benzanthrone Dyes and Lysozyme Amyloid Fibrils. *J. Fluoresc.* **2014**, *24*, 493−504.
(18) Siddlingeshwar, B.; Hanagodimath, S. M.; Kirilova, E. M.; Kirilov, G. K. Photophysical characteristics of three novel benzanthrone derivatives: Experimental and theoretical estimation of dipole moments. *J. Photochem. Photobiol., B* **2011**, *112*, 448−456.
(19) Ryzhova, O.; Vus, K.; Trusova, V.; Kirilova, E.; Kirilov, G.; Gorbenko, G.; Kinnunen, P. Novel benzanthrone probes for membrane and protein studies. *Methods Appl. Fluoresc.* **2016**, *4*, 034007.
(20) Kapusta, P.; Machalický, O.; Hrdina, R.; Nepraš, M.; Zimmt, M. B.; Fidler, V. Photophysics of 3-Substituted Benzanthrones: Substituent and Solvent Control of Intersystem Crossing. *J. Phys. Chem. A* **2003**, *107*, 9740−9746.
(21) Adamo, C.; Jacquemin, D. The calculations of excited-state properties with Time-Dependent Density Functional Theory. *Chem. Soc. Rev.* **2013**, *42*, 845−856.
(22) Trusova, V. M.; Kirilova, E.; Kalnina, I.; Kirilov, G.; Zhytniakivska, O. A.; Fedorov, P. V.; Gorbenko, G. P. Novel Benzanthrone Aminoderivatives for Membrane Studies. *J. Fluoresc.* **2012**, *22*, 953−959.
(23) Frisch, M. J.; et al. *Gaussian 09*, Revision D.01; Gaussian Inc.: Wallingford CT, 2009.
(24) Yanai, T.; Tew, D. P.; Handy, N. C. A new hybrid exchange−correlation functional using the Coulomb-attenuating method (CAM-B3LYP). *Chem. Phys. Lett.* **2004**, *393*, 51−57.
(25) (a) Perdew, J. P.; Burke, K.; Ernzerhof, M. Generalized gradient approximation made simple. *Phys. Rev. Lett.* **1996**, *77*, 3865−3868. (b) Perdew, J. P.; Burke, K.; Ernzerhof, M. Errata: Generalized gradient approximation made simple. *Phys. Rev. Lett.* **1997**, *78*, 1396. (c) Adamo, C.; Barone, V. Toward reliable density functional methods without adjustable parameters: The PBE0 model. *J. Chem. Phys.* **1999**, *110*, 6158−6170.
(26) (a) Grimme, S.; Antony, J.; Ehrlich, S.; Krieg, H. A consistent and accurate ab initio parameterization of density functional dispersion correction (DFT-D) for the 94 elements H-Pu. *J. Chem. Phys.* **2010**, *132*, 154104. (b) Grimme, S.; Ehrlich, S.; Goerigk, L. Effect of the damping function in dispersion corrected density functional theory. *J. Comput. Chem.* **2011**, *32*, 1456−1465.
(27) Weigend, F.; Ahlrichs, R. Balanced basis sets of split valence, triple zeta valence and quadruple zeta valence. *Phys. Chem. Chem. Phys.* **2005**, *7*, 3297.
(28) Shivraj, S.; Siddlingeshwar, B.; Kirilova, E. M.; Belyakov, S. V.; Divakar, D. D.; Alkheraif, A. A. Photophysical properties of benzanthrone derivatives: effect of substituent, solvent polarity and hydrogen bonding. *Photochem. Photobiol. Sci.* **2018**, *17*, 453−464.
(29) (a) Miertuš, S.; Scrocco, E.; Tomasi, J. Electrostatic Interaction of a Solute with a Continuum. A Direct Utilization of ab initio Molecular Potentials for the Prevision of Solvent Effects. *Chem. Phys.* **1981**, *55*, 117−129. (b) Miertuš, S.; Tomasi, J. Approximate Evaluations of the Electrostatic Free Energy and Internal Energy Changes in Solution Processes. *Chem. Phys.* **1982**, *65*, 239−245. (c) Pascual-Ahuir, J. L.; Silla, E.; Tuñon, I. GEPOL: An improved description of molecular-surfaces. 3. A new algorithm for the computation of a solvent-excluding surface. *J. Comput. Chem.* **1994**, *15*, 1127−1138. (d) Cossi, M.; Barone, V.; Cammi, R.; Tomasi, J. Ab initio study of solvated molecules: A new implementation of the polarizable continuum model. *Chem. Phys. Lett.* **1996**, *255*, 327−335. (e) Barone, V.; Cossi, M.; Tomasi, J. A new definition of cavities for the computation of solvation free energies by the polarizable continuum model. *J. Chem. Phys.* **1997**, *107*, 3210−3221. (f) Cancès, E.; Mennucci, B.; Tomasi, J. A new integral equation formalism for the polarizable continuum model: Theoretical background and applications to isotropic and anistropic dielectrics. *J. Chem. Phys.* **1997**, *107*, 3032−3041. (g) Mennucci, B.; Tomasi, J. Continuum solvation models: A new approach to the problem of solute's charge distribution and cavity boundaries. *J. Chem. Phys.* **1997**, *106*, 5151−5158. (h) Mennucci, B.; Cancès, E.; Tomasi, J. Evaluation of Solvent Effects in Isotropic and Anisotropic Dielectrics and in Ionic Solutions with a Unified Integral Equation Method: Theoretical Bases, Computational Implementation and Numerical Applications. *J. Phys. Chem. B* **1997**, *101*, 10506−10517. (i) Barone, V.; Cossi, M. Quantum calculation of molecular energies and energy gradients in solution by a conductor solvent model. *J. Phys. Chem. A* **1998**, *102*, 1995−2001. (j) Cossi, M.; Barone, V.; Mennucci, B.; Tomasi, J. Ab initio study of ionic solutions by a polarizable continuum dielectric model. *Chem. Phys. Lett.* **1998**, *286*, 253−260. (k) Barone, V.; Cossi, M.; Tomasi, J. Geometry optimization of molecular structures in solution by the polarizable continuum model. *J. Comput. Chem.* **1998**, *19*, 404−417. (l) Cammi, R.; Mennucci, B.; Tomasi, J. Second-order Møller-Plesset analytical derivatives for the polarizable continuum model using the relaxed density approach. *J. Phys. Chem. A* **1999**, *103*, 9100−9108. (m) Cossi, M.; Barone, V.; Robb, M. A. A direct procedure for the evaluation of solvent effects in MC-SCF calculations. *J. Chem. Phys.* **1999**, *111*, 5295−5302. (n) Tomasi, J.; Mennucci, B.; Cancès, E. The IEF version of the PCM solvation method: An overview of a new method addressed to study molecular solutes at the QM ab initio level. *J. Mol. Struct.: THEOCHEM* **1999**, *464*, 211−226. (o) Cammi, R.; Mennucci, B.; Tomasi, J. Fast evaluation of geometries and properties of excited molecules in solution: A Tamm-Dancoff model with application to 4-dimethylaminobenzonitrile. *J. Phys. Chem. A* **2000**, *104*, 5631−5637. (p) Cossi, M.; Barone, V. Solvent effect on vertical electronic transitions by the polarizable continuum model. *J. Chem. Phys.* **2000**, *112*, 2427−2435. (q) Cossi, M.; Barone, V. Time-dependent density functional theory for molecules in liquid solutions. *J. Chem. Phys.* **2001**, *115*, 4708−4717. (r) Cossi, M.; Rega, N.; Scalmani, G.; Barone, V. Polarizable dielectric model of solvation with inclusion of charge penetration effects. *J. Chem. Phys.* **2001**, *114*, 5691−5701. (s) Cossi, M.; Scalmani, G.; Rega, N.; Barone, V. New developments in the polarizable continuum model for quantum mechanical and classical calculations on molecules in solution. *J. Chem. Phys.* **2002**, *117*, 43−54. (t) Cossi, M.; Rega, N.; Scalmani, G.; Barone, V. Energies, structures and electronic properties of molecules in solution with the C-PCM solvation model. *J. Comput. Chem.* **2003**, *24*, 669.
(30) Tomasi, J.; Mennucci, B.; Cammi, R. Quantum mechanical continuum solvation models. *Chem. Rev.* **2005**, *105*, 2999−3094.
(31) Marenich, A. V.; Cramer, C. J.; Truhlar, D. G. Universal solvation model based on solute electron density and a continuum model of the solvent defined by the bulk dielectric constant and atomic surface tensions. *J. Phys. Chem. B* **2009**, *113*, 6378−6396.
(32) Dennington, R.; Keith, T.; Millam, J. *GaussView*, Version 5.0.9; Semichem Inc.: Shawnee Mission, KS, 2009.
(33) Krasovitskii, B. M.; Bolotin, B. *Organic Luminophores*; Khimiya: Moscow, 1984; Vol. *1230*.
(34) Demchenko, A. P. *Introduction to Fluorescence Sensing*; Springer Science & Business Media, 2008.
(35) Beyhan, S. M.; Götz, A. W.; Ariese, F.; Visscher, L.; Gooijer, C. Computational Study on the Anomalous Fluorescence Behavior of Isoflavones. *J. Phys. Chem. A* **2011**, *115*, 1493−1499.


https://doi.org/10.1021/acsomega.1c05849
*ACS Omega* 2021, 6, 32334−32341

(36) Weissleder, R.; Ntziachristos, V. Shedding light onto live molecular targets. *Nat. Med.* **2003**, *9*, 123−128.



https://doi.org/10.1021/acsomega.1c05849
*ACS Omega* 2021, 6, 32334−32341